Journal Name

ARTICLE

A quantitative measure of halogen bond activation in cocrystallization

Lucia Carlucci* and Angelo Gavezzotti*

A theoretical investigation of bond lengths and bond energies for several kinds of halogen bonding interactions is carried out by the PIXEL method. The effect of different kinds of activating agents, fluoro-, nitro-, ethynyl substitution and combinations thereof, is assessed quantitatively, and is found to be fully consistent with the results of literature screenings of the corresponding strengths, as judged by the ease of formation of cocrystals. In the best combination of activators the halogen bond is comparable or superior to a strong O-H...O hydrogen bond in what concerns stabilization energies and stretching force constants. At least with iodine acceptors, in our picture the halogen-bonding effect is a localized interaction arising from detail of the electron distribution at the halogen atom, mainly of a Coulombic-polarization nature but with dispersion energies contributing significantly. Binding energies correlate with the electrostatic potential at the tip of the halogen and even with Mulliken population analysis atomic charges, providing easily accessible guidelines for crystal engineers. For one typical cocrystal structure the analysis of separate molecule-molecule energies reveals the nature of the packing forces and rank halogen bonding as the main influence, closely followed by coplanar stacking of coformers.

Received 00th January 20xx,
Accepted 00th January 20xx

DOI: 10.1039/x0xx00000x

www.rsc.org/

1. Introduction

Halogen bonding (XB) was originally discovered and denominated in small inorganic molecular systems,[1] but has recently been defined by IUPAC[2a] and extensively exploited for the study of intermolecular interaction in organic molecules.[2] The essentials of the interaction physics are an attraction and subsequent stabilization by contact between an electron-rich donor terminus, a basic nitrogen or oxygen atom, and an acidic electron-hole site at the front of a halogen atom along the extension of the C-X bond. The strength of XB increases on going from chlorine to bromine to iodine, and with appropriate substitution. Cohesive energies go from nearly zero in unsubstituted Cl...O contacts to some 30 kJ mol^{-1} in activated I...N systems,[3] in the latter case competing with a medium-strong O-H...O hydrogen bond.

Strategies for the increase of the σ-hole, *i.e.* depletion of electron density at the halogen atom (XB donor) have been explored mainly in two ways: i) by increasing the *s* character and then the electronegativity of the carbon atom to which the halogen atom is attached; ii) by increasing the electron-withdrawing ability of the fragments bearing the halogen atom. Iodoethynyl-containing molecules are particularly suitable to be cocrystallized with nitrogen and oxygen-based XB acceptors.[4,5] Such activated XB has been also exploited to organize iodo-polyacethylene molecules for topochemical solid-state polymerization.[6] Strongly electron-withdrawing fluorine and nitro groups are candidates to activate XB donor molecules: fluorinated haloaromatics[7] and haloaliphatics[8] have been extensively used in cocrystallization with different XB acceptors. The XB strength in fluorinated diiodobenzene can be modulated by the number of fluorine atoms, in an additive manner.[9] Examples of nitro group activation have been reported.[10,11] More recently stronger XBs have been obtained by double activation, i.e. by fluoro or nitro substitution along with halogen (iodine or bromine) attached to ethynyl groups.[12,13] An increase of the σ-hole at the halogen can be also achieved by protonation or alkylation, with halogen-substituted pyridyl groups.[14]

A special case of exploitation of XB is the selective or competitive formation of cocrystals between donor- and acceptor-carrying compounds.[15] In a systematic study of cocrystallization of substituted iodobenzenes with aza-aromatics[16] the effect of activation has been directly gauged by the selective formation of the corresponding cocrystal. Theoretical investigations of XB have been carried out at many levels of theory, and the resulting, conspicuous literature may

[a] *Dipartimento di Chimica, Università degli Studi di Milano, via C. Golgi 19, 20133 Milano, Italy. Email: lucia.carlucci@unimi.it, angelo.gavezzotti@unimi.it*

† Electronic Supplementary Information (ESI) available: full Tables of average bond lengths and distribution curves, calculated bond energy profiles. See DOI: 10.1039/x0xx00000x

be found in a thorough account previously given[2c]. The case with iodobenzene-azaaromatic cocrystals is exemplary and provides the ideal basis for a concomitant theoretical study. We report in this paper some results that support and rationalize the qualitative experimental findings, and offer a quantitative estimate of the involved activation effects. Such result help clarifying physics fundamentals and may serve as guidelines to experiment.

2 Methods

Crystal data retrievals were carried out using Cambridge Crystallographic Data Center (CCDC) software in the informatics system that frames the Crystal Structure Database, CSD.[17] For crystal structure calculations H-atom positions were recalculated according to standardized procedures.[3,18] Energy calculations are performed in the PIXEL environment[3,18] on some relevant crystal structures[16] and on the selected dimer systems shown in Scheme 1. For these model compounds molecular dimensions are taken from known structures[16] or from average bond lengths and angles from the CSD (see ESI, Table S1). Electron density grids are obtained at the MP2/DGDZVP level of theory. Due to the space extension of the large iodine electron density, all PIXEL numerical integration procedures are put to an unusual strain. Therefore a finer step had to be used for the grids (0.06 rather than the usual 0.08 Å). Original density units (whose number is of the order of 2 x 10^6) are then contracted into *n* x *n* x *n* super-cubes, with n = 4 rather than the usual n = 3 in order to keep the final number of contracted density units within a reasonable range (< 50,000) for the actual integrations; *n* = 4 reduces the computing time for a full binding energy curve from 90 to 40 minutes. Spot tests carried out using n = 2 or 3 and/or different grid steps showed minor (< 10%) differences in absolute energy values but invariably no difference in relative energy ranks, which are what counts in assessing the relative cohesive efficiencies.

The cohesive energy of the dimers in Scheme 1 is calculated between rigid frameworks by changing the halogen-nitrogen distance between 2.5 and 4.0 Å in steps of 0.1 Å. Minor numerical fluctuations in overlap integrals were mitigated by smoothing the overlap repulsion vs. distance curves by fitting to a fourth-order polynomial. The cohesive energy curves E(R) are then re-fitted with a third-order polynomial where dE/dR = 0 provides the equilibrium distance, R°, and the well depth or cohesive energy, E°, while k° = (d^2E/dR^2)° is a formal bond stretching force constant.

Thanks to the flexibility of the PIXEL formalism all calculations can be comfortably carried out on laptop computers. The reliability of the obtained numbers has been repeatedly assessed by comparison with high-level *ab initio* calculations.[3,19]

3 Results and discussion

a) Overview. Table 1 and Figures 1-3 provide an overview of the energy results for the molecular dimers. It is known that increasing the s character at the carbon atom of the C-X center strengthens the XB interaction. In fact we find that substituting a methyl group (iodomethane) with a phenyl ring (iodobenzene) does shorten the I...N contact distance (Table 1), although this substitution does not enhance the interaction energy. It is to be expected that the XB would be stronger with an iodoacetylene donor. On the other hand, while perfluoro substitution brings about a significant stabilization (Figure 1a).

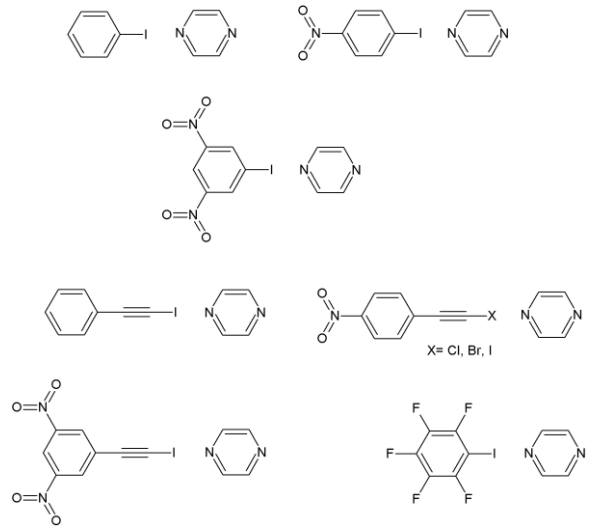

Scheme 1 Model dimers with pyrazine: iodobenzene (Bz-I), 4-nitroiodobenzene (4NBz-I), 3,5-dinitro iodobenzene (3,5NBz-I), iodoethynylbenzene (BzEt-I), 4-nitrohaloethynylbenzene (halogen = I, 4NBzEt-I; Br, 4NBzEt-Br; Cl, 4NBzEt-Cl), 3,5,-dinitroiodoethynylbenzene (3,5NBzEt-I), pentafluoroiodobenzene (FBz-I).

Table 1 Cohesion parameters for molecular dimers of several XB donors with pyrazine.

donor	R°, Å % reduction	E°, kJmol^{-1}	k°, kJmol^{-1}Å^{-2}	U,[b] kJmol^{-1}	q(I)[c]
CH_3-I[a]	3.15 -14%	-15.1	92	-	-0.047
Bz-I n=4	3.09 -16	-15.1	122	103	-0.059
n=3	3.12 -15	-13.6	-	-	-
4NBz-I	3.08 -16	-18.3	125	-	-0.010
3,5NBz-I	3.03 -17	-24.4	121	165	+0.031
FBz-I	3.07 -16	-23.5	104	166	+0.091
BzEt-I	2.99 -18	-25.1	117	157	+0.035
4NBzEt-I	2.95 -20	-30.2	196	189	+0.054
3,5NBzEt-I	2.97 -19	-29.5	155	206	+0.072
4NBzEt-Br	3.13 -11	-15.0	160	-	-
4NBzEt-Cl	3.17 -7	-9.9	97	-	-

a) Equilibrium X...N distance, % reduction over sum of atomic radii (N 1.64, I 2.03, Br 1.87, Cl 1.76), cohesive energy and formal bond stretching constant. b) Electrostatic potential at iodine atom.[16] c) Mulliken population charge on the iodine atom from the MO calculation.

As in many previous experiences, changing the contraction level from *n* = 4 (used throughout) to *n* = 3 changes the interaction energies by a constant factor of 0.90 to 0.95 (Figure

1b). Nitro substitution on the phenyl ring consistently shortens the contact distance and increases the bond energy (Figure 2); dinitro and pentafluoro substitution have a comparable effect. Attaching the iodine atom to an ethynyl group is highly effective, iodoethynylbenzene being even a better donor that dinitroiodobenzene. Then, introduction of nitro substituents on the iodoethynyl system has a further bond enhancing effect, although mono- and dinitro substitution appear to be more or less equivalent (Figure 3a). The ethynyl group activation makes the Br...N contact barely bonding, while not even ethynyl group activation can turn chlorine into an effective XB donor (Figure 3b).

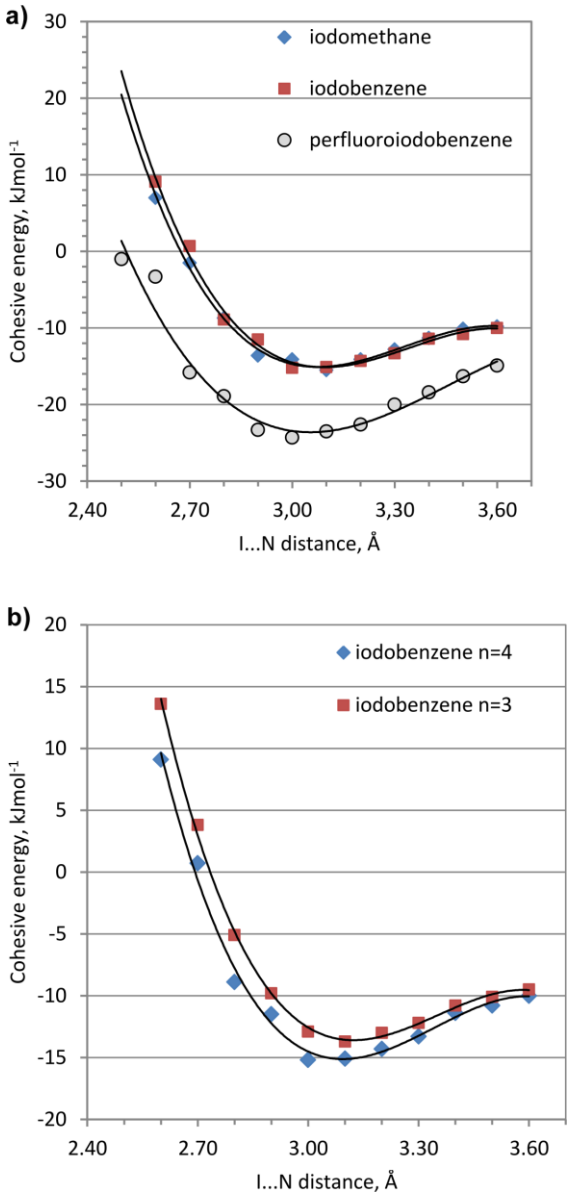

Figure 1 (a) Binding potential energy curves for dimers of pyrazine with iodomethane, iodobenzene and perfluoroiodobenzene showing the significant stabilization effect of fluoro substituents. (b) Effect of changing the contraction level of calculation on the binding potential energy curve for the pyrazine iodobenzene dimer.

The calculated I...N bond lengths of the XB interactions compare rather favorably with those observed in the corresponding cocrystals, with an average lengthening of a few percent e.g. exptl. KUXBIQ[16] 2.71, KUXBEM[16] 2.74, calc. 4NBzEt-I 2.95; exptl. KUWNEX[16] 2.93, calc. 3,5NBzEt-I 2.97 Å. The binding force constants k° provide a rough estimate of the flexibility of the corresponding bonds. In a harmonic approximation, as in ordinary chemical bonds, $E = 1/2k°(R-R°)^2$. At the cost of the room temperature value of *RT* (2.5 kJ mol^{-1}) a bond with k° = 100, 150 and 200 kJ mol^{-1} Å^{-2} has a free oscillation of 0.44, 0.36 and 0.32 Å respectively. For comparison, O-H...O or O-H...N hydrogen-bond binding energies are 25-40 kJ mol^{-1} and force constants under the same approximation are of the order of 150-300 kJ mol^{-1} Å^{-2} while covalent C-C force constants are of the order of 3000-4000 kJ mol^{-1} Å^{-2}.[20] In this picture, halogen bonds appear as rather fluxional systems, so that only the most activated ones are as rigid as a conventional hydrogen bond.

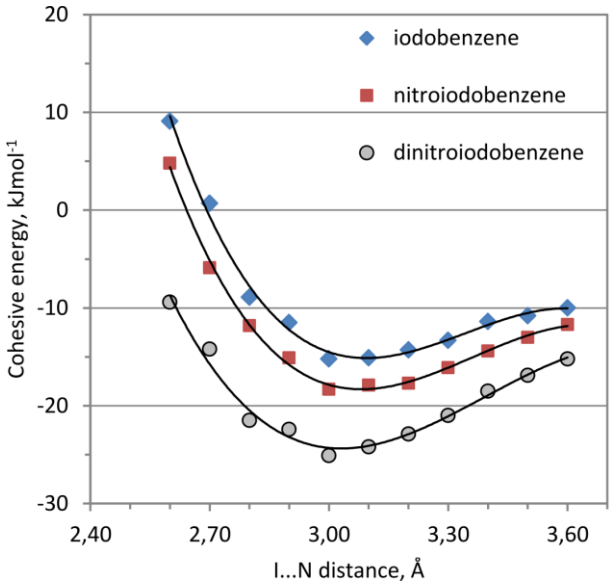

Figure 2. Effect of nitro substitution on the binding potential energy curves for the dimers shown in Scheme 1.

The chemical identity of halogen-bonding effects can be understood using the energy breakdown into Coulomb-polarization, dispersion-repulsion terms (Table 2). Dispersion energy is constant for all substituents, from a methyl group to a dinitroethynyl group. The increase in binding energy with increasingly activating substituents at the phenyl ring depends mainly on small increases in Coulomb-polarization energy, as expected: an electrostatic, sigma-hole effect. Perhaps surprisingly, activating groups also bring about a decrease in repulsion energy. Recalling that in our approach the repulsion energy is modeled as a Pauli-overlap effect, the observed repulsion decrease must arise from withdrawal of electrons from the surroundings of the C-I...N< binding site, a further sigma-hole effect. While one is never careful enough in drawing such conclusions on electronic effects from model calculations, it may be reminded that the PIXEL energy partitioning compares favorably with the breakdown resulting from first-principles *ab initio* (SAPT) calculations.[21]

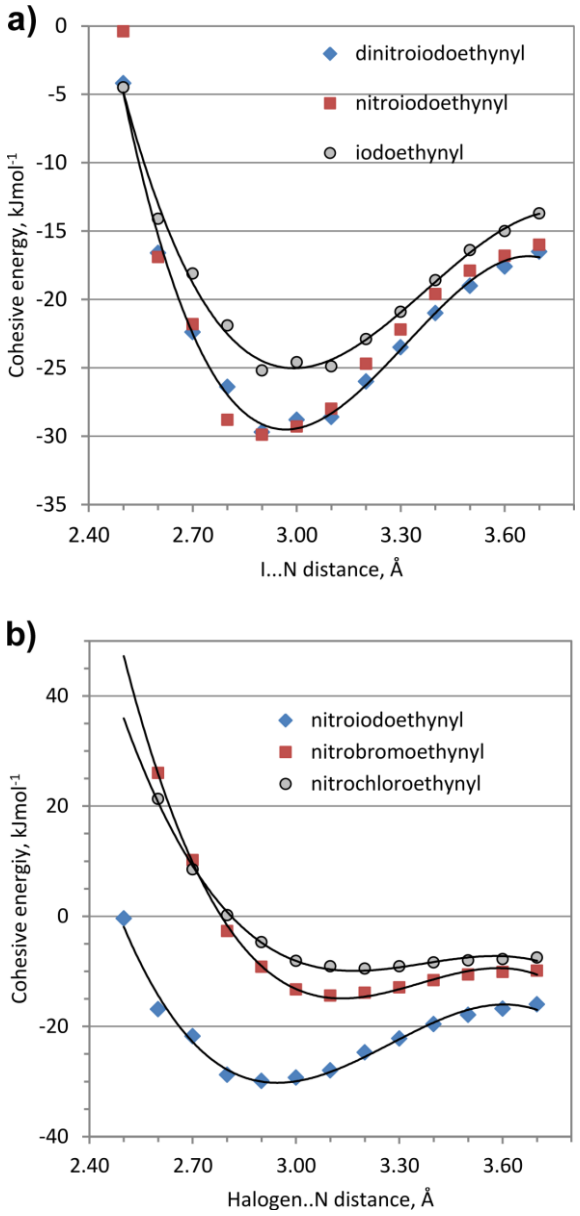

Figure 3. Binding potential energy curves for the XB interaction of some dimers in Scheme 1, as a function of I...N distance. The acceptor is always pyrazine.

b) Halogen-bonding factors. The collective interpretation of the above results suggests that the halogen-bonding effect, in terms of Coulombic and repulsion energies, is indeed a matter of the electron distribution at the C-I...N< environment and, since the acceptor is always the same, a matter of fine detail of the electron distribution at the iodine atom. Dispersion contributions are on the contrary quite insensitive to that detail, in agreement with the scarcely directional nature of the dispersive interaction. Dispersion does not seem to depend on substituents and is therefore also localized on the binding environment. It should be remembered that dispersion anyway provides a non-negligible component of the intermolecular binding effect along with Coulombic force.

Table 2 Energy breakdown for the halogen-bond complexes in Scheme 1 at halogen...N separation of 3.1 Å.

donor	E(coul+pol)	E(disp)	E(rep)[a]	E(tot)
CH_3-I	-40.0	-14.2	39.7	-14.6
Bz-I	-39.9	-14.5	40.1	-14.3
4NBz-I	-41.3	-14.7	38.1	-17.9
3,5NBz-I	-46.0	-14.7	36.3	-24.3
FBz-I	-44.7	-14.3	35.4	-23.6
BzEt-I	-45.3	-14.1	34.2	-25.3
4NBzEt-I	-47.4	-14.2	35.3	-26.2
3,5NBzEt-I	-48.6	-14.3	34.8	-28.0
4NBzEt-Br	-26.4	-9.3	22.1	-13.6
4NBzEt-Br	-17.6	-8.3	17.6	-8.4

a) Uncorrected repulsion energies before polynomial fitting. Differences with fitted values never exceed 1.5 kJ mol^{-1}.

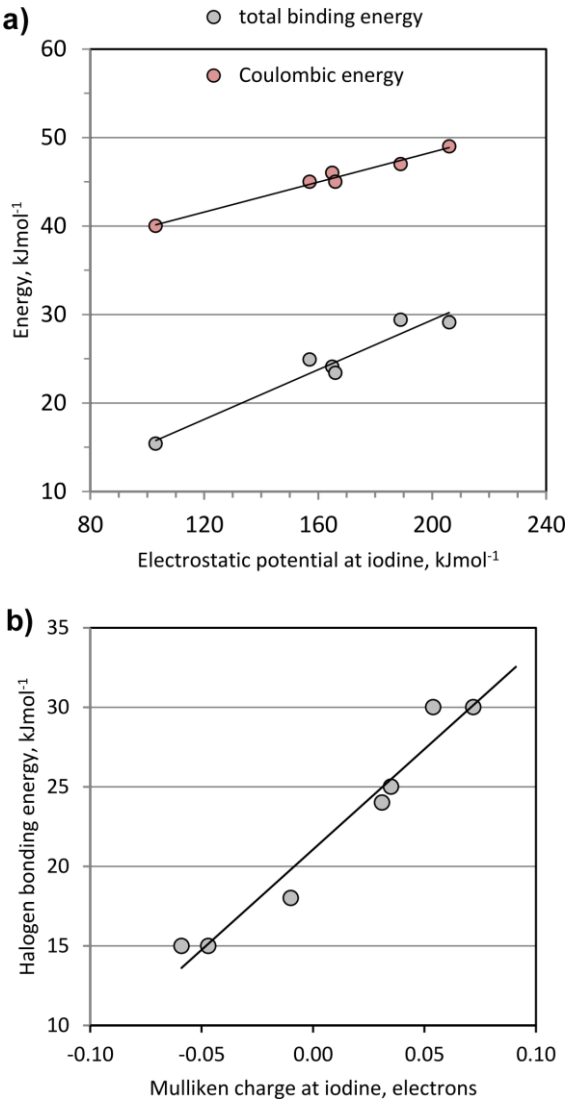

Figure 4. (a) Total binding energy and Coulombic-polarization energies as a function of electrostatic potentials (kJ mol^{-1}) at the iodine atom. Potentials are from ref. 16. (b) Halogen-bonding total interaction energy as a function of Mulliken charge at the iodine atom (not including pentafluoroiodobenzene).

A further hint for the physical interpretation of XB is provided by the linear plot of Coulombic-polarization energy and total binding energy as a function of the electrostatic potential at the tip of the iodine atom (Figure 4a). Widely different substitution patterns provide nearly identical electrostatic potentials and interaction energies. With the exception of pentafluoro derivative, also a very simple indicator like the net charge at the iodine atom resulting from a Mulliken population analysis on the MP2 wavefunction shows a good correlation with binding energies (Figure 4b). These plots provide some simple quantitative guidelines for crystal engineering: the strength of the I...N interaction energy is comparable to that of a classical O,N-H...O,N hydrogen bonds for a peripheral potential of at least 150 kJ mol^{-1} at the iodine atom.

c) Cocrystallization. Further energy calculations provide insights into the structure-driving influence of XB in cocrystallization. For a case study we consider the very typical crystal structure of the iodoethynyl-4-nitrobenzene cocrystal with 4-(phenylendiazenyl)pyridine (CSD refcode KUXBIQ).[16] The most conspicuous feature of the structure has linear halogen-bonded dimers, stacked head to tail (Figure 5). Intermolecular energies within this structure were calculated by PIXEL, subdivided into molecule-molecule contributions, in order to assess which molecular pairs mostly contribute to the lattice stability.

Numerical results are collected in Table 3 with pictorial representations in Figures 6. The halogen-bonded dimer is the top-ranking structure determinant with a very large Coulombic-polarization contribution, as expected, and a total cohesive energy more or less equivalent to a medium-strong hydrogen bond. The large repulsive term reveals a large overlap between the very extended iodine electron cloud and the nitrogen atom.

Next in importance are two offset stacked, or almost coplanar-parallel, pairs of iodoethynyl molecules (Figure 6, B, C). An offset pair of diazenylpyridines (F) provides a fourth-ranking stabilization. A further, weaker stabilizing pair (D) shows what appears as a stacked interaction between the iodine atom and the triple bond, somewhat counter-intuitive as it involves a contact between two electron-rich moieties.

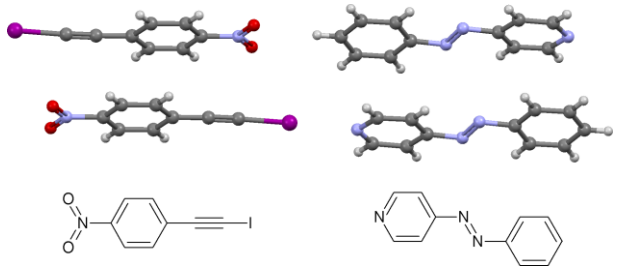

Figure 5 The halogen-bonding plus stacking feature in the crystal structure of the iodoethynyl-4-nitrobenzene, 4-(phenylendiazenyl)pyridine cocrystal.[16] The I...N distance is 2.71 Å.

Table 3 Molecule-molecule energies in the crystal structure of the iodoethynyl-4-nitrobenzene cocrystal with 4-(phenylendiazenyl)pyridine (Refcode: KUXBIQ[a]).[16]

	E(c)	E(d)	E(r)	E(t)	interaction type	symmetry
halogen bond	-144	-27	140	-32	I...N 2.71 Å	x,y,z
iodoethynyl	-39 -23	-45 -30	77 31	-8 -21	full pi-stack, **A** lateral 1, **B**	2-x,2-y,1-z 2-x,1-y,1-z
iodoethynyl	-16	-22	23	-16	lateral 2, **C**	1-x,2-y,1-z
iodoethynyl	-18	-23	31	-10	inverted C≡C-I, **D**	1-x,1-y,1-z
diazenyl-pyridine	-26 -18	-44 -26	61 30	-8 -14	full stack, **E** offset stack, **F**	-x,1-y,-z -x,-y,-z

a) Crystal structure is in Space Group P-1 with one full dimer in asymmetric unit.

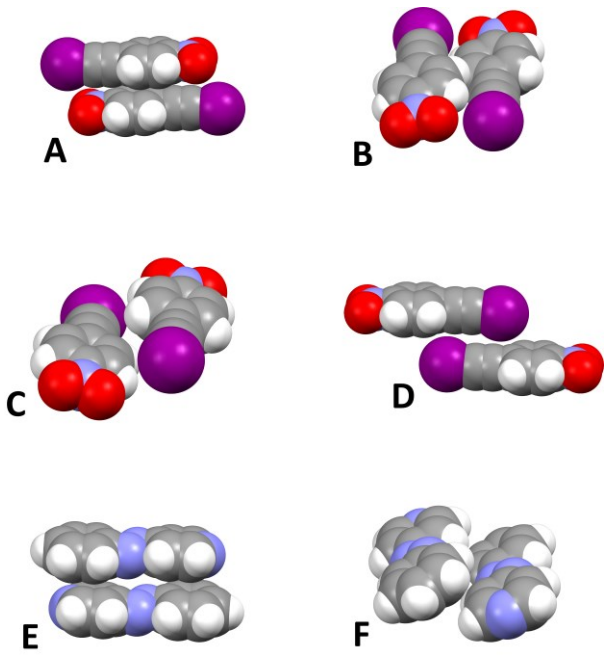

Figure 6 CPK representations of the six **A**-**F** interaction types described in Table 3. **A**: centroid-centroid distance (Cg…Cg) = 3.64 Å; mean plane to mean plane distance (mpl…mpl) = 3.42 Å; mean plane to mean plane angle (mpl∠mpl) = 0°. **B**: Cg…Cg = 6.25 Å; mpl…mpl = 2.20 Å; mpl∠mpl = 0°; I…I distance = 9.49 Å. **C**: Cg…Cg = 7.59 Å; mpl…mpl = 1.68 Å; mpl∠mpl = 0°; I…I distance=8.28 Å. **D**: Cg…Cg = 9.52 Å; mpl…mpl =3.94 Å; mpl∠mpl = 0°; I…I distance = 5.23 Å. **E**: Cg…Cg = 3.79 Å; mpl∠mpl = 7.4°. **F**: Cg…Cg = 5.78 Å; mpl∠mpl = 7.4°. A complete view of the six interaction types in the unit cell is shown in Figure S1.

Rather surprisingly, the two fully stacked pairs (A and E) are only marginally stabilizing, with a substantial dispersive stabilization countered by a large overlap repulsion. The effect appears in the stacking of both coformers, so it may not be a shortcoming of the parameterization; in particular, the base is a light-atom moiety for which the PIXEL performance is well documented. A provisional conclusion is that in the overall stabilization of the crystal structure, other, stronger forces prevail, and these stacked dimers are somewhat compressed into a less favorable or slightly unfavorable arrangement.

Remarkably, the base coformer itself (CSD refcode QUFDIG) has a disordered crystal structure without ring stacking.[22]

4. Conclusions

PIXEL calculations on model systems clearly reveal the relative effects of chemical substitution on the stability and cohesive energy of halogen-bonded dimers. Nitro substitution and perfluoro substitution are important, but anchoring the iodine atom to an ethynyl group is even more effective as found experimentally.[16] Stabilizing effects are to a certain extent additive, certainly so for nitro and ethynyl substitution, apparently less so for double nitro vs. single nitro substitution. The effects are quantitatively measured by the resulting calculated cohesive energies: within the structural set examined here, the extremes are 9.9 kJ mol^{-1} for a nitro-chloro donor, barely worth the denomination of a bond, to about 30 kJ mol^{-1} for the top activated, nitroethynyl iodo derivatives. A linear relationship is found for the cohesive energy with the electrostatic potential at the tip of the iodine atoms, and even with a simple indicator as the total atomic charge from a Mulliken population analysis, providing clearly identifiable and readily available guidelines for making crystal engineering efforts more quantitative. The PIXEL energy partitioning confirms (if need be, but quantitatively) that the XB is a localized interaction at the I...N site mainly driven by Coulombic effects between the sigma hole and the basic nitrogen electrons. The large and diffuse iodine electron cloud provides also a non-negligible contribution in terms of dispersion energies.

The results of model systems match very well the outcome of systematic cocrystallization experiments: only those cocrystals for which the corresponding model system shows a significant activation are actually observed.[16] This post-diction can hopefully be turned into a valuable tool for prediction, also considering that PIXEL calculations are a readily available carrier of information without recourse to specialized theoretical chemistry or supercomputing. Confidence in the results is increased by a good agreement between observed and calculated I...N distances.

The analysis of packing drives in a typical halogen bonded cocrystal reveal that the super-activated iodoethynyl...nitrogen contact is responsible for the primary aggregation of the coformers into a cocrystallization pair, with a dimerization stabilization of 32 kJ mol^{-1} or the equivalent of a strong structure-driving hydrogen bond. Contrary to expectation, ring stacking does not offer a significant contribution; a possible interpretation of this fact is that the bulk of the iodine atom together with the primary requirements of its arranging itself into the XB, prevail over what is normally a predominant feature of the crystal packing of flat aromatic compounds.

References

1 A. C. Legon, *Angew. Chem. Int. Ed.*, 1999, **38**, 2686-2714.

2 (a) G. R. Desiraju, P. S. Ho, L. Kloo, A. C. Legon, R. Marquardt, P. Metrangolo, P. Politzer, G. Resnati and K. Rissanen, *Pure Appl. Chem*., 2013, **85**, 1711–1713. (b) C. B. Aakeröy, C. L. Spartz, S. Dembowski, S. Dwyrea and J. Desper, *IUCrJ*, 2015, **2**, 498-510; (c) G. Resnati, E. Boldyreva, P. Bombicz and M. Kawano, *IUCrJ*, 2015, **2**, 675-690; (d) L. C. Gilday, S. W. Robinson, T. A. Barendt, M. J. Langton, B. R. Mullaney and Paul D. Beer, *Chem. Rev*., 2015, **115**, 7118-7195; (e) M. J. Langton, S. W. Robinson, I. Marques, V. Félix and P.D Beer, *Nat. Chem.*, 2014, **6**, 1039–1043; (f) G. Cavallo, P. Metrangolo, R. Milani, T. Pilati, A. Priimagi, G. Resnati and G. Terraneo, *Chem. Rev*., 2016, **116**, 2478–2601.

3 A. Gavezzotti, *Mol. Phys*., 2008, **106**, 1473-1485.

4 C. Perkins, S. Libri, H. Adams and L. Brammer, *CrystEngComm*, 2012, **14**, 3033-3038.

5 L. Gonzalez, N. Gimeno, R. M. Tejedor, V. Polo, M. B. Ros, S. Uriel and J. L. Serrano, *Chem. Mater*., 2013, **25**, 4503–4510.

6 (a) N. S. Goroff, S. M. Curtis, J. A. Webb, F. W. Fowler and J. W. Lauher, *Org. Lett*., 2005, **7**, 1891-1993; (b) J. W. Lauher, F. W. Fowler andN. S. Goroff, *Acc. Chem. Res*., 2008, **41**, 1215–1229.

7 M. Saccone, G. Cavallo, P. Metrangolo, A. Pace, I. Pibiri, T. Pilati, G. Resnati and G. Terraneo, *CrystEngComm*, 2013, **15**, 3102–3105.

8 R. B. Walsh, C. W. Padgett, P. Metrangolo, G. Resnati, T. W. Hanks and W. T. Pennington, *Cryst. Growth Des*., 2001, **1**, 165–175.

9 C. Präsang, A. C. Whitwood, and Duncan W. Bruce, *Crystal Growth Des*., 2009, **9**, 5319–5326.

10 N. R. Goud, O. Bolton, E. C. Burgess and Adam J. Matzger, *Cryst. Growth Des*., 2016, **16**, 1765–1771.

11 K. Raatikainen and K. Rissanen, *CrystEngComm*, 2009, **11**, 750–752.

12 E. Bosch *Cryst. Growth Des*. 2014, **14**, 126–130.

13 S. T. Nguyen, A. L. Rheingold, G. S. Tschumper, and D. L. Watkins, *Cryst. Growth Des*., 2016, **16**, 6648–6653.

14 T. A. Logothetis, F. Meyer, P. Metrangolo, T. Pilati, G. Resnati, *New J. Chem*., 2004, **28**, 760–763.

15 (a) T. Friščić and W. Jones, *Crystal Growth Des*., 2009, **9**, 1621–1637; (b) S. d'Agostino, F. Grepioni, D. Braga and B. Ventura, *Cryst. Growth Des*., 2015, **15**, 2039–2045; (c) C. B. Aakeröy, M. Baldrighi, J. Desper, P. Metrangolo and G. Resnati, *Chem. Eur. J*., 2013, **19**, 16240 – 16247.

16 C. B. Aakeröy, T. K. Wijethunga, J. Desper and M. Dakovic, *Cryst.Growth Des*., 2015, **15**, 3853-3861.

17 C. R. Groom, I. J. Bruno, M. P. Lightfoot and S. C. Ward, *Acta Cryst*., 2016,. **B72**, 171-179.

18 A. Gavezzotti, *New J. Chem*., 2011, **35**, 1360-1368. Unless otherwise stated all procedures and software for data handling downstream of CSD, including source codes and complete documentation, are available for consultation and download from the CLP section at www.angelogavezzotti.it.

19 L. Maschio, B. Civalleri, P. Ugliengo and A. Gavezzotti, *J. Phys. Chem*. *A*, 2011, **115**, 11179-11186.

20 A.Gavezzotti, *New J. Chem*., 2016, **40**, 6848-6853.

21 S. A. Moggach, W. G. Marshall, D. M. Rogers and S. Parsons, *CrystEngComm*, 2015 , **17**, 5315.

22 K. M. Hutchins, R. H. Groeneman, E. W. Reinheimer, D. C. Swenson, L. R. MacGillivray, *Chem. Sci*., 2015, **6**, 4717-4722.